MOLECULAR
METABOLISM

Mitochondrial Dynamin-Related Protein 1 (DRP1) translocation in response to cerebral glucose is impaired in a rat model of early alteration in hypothalamic glucose sensing

Lucie Desmoulins [1], Chloé Chrétien [1], Romain Paccoud [1], Stephan Collins [1], Céline Cruciani-Guglielmacci [2,3], Anne Galinier [4], Fabienne Liénard [1], Aurore Quinault [1], Sylvie Grall [1], Camille Allard [1], Claire Fenech [1], Lionel Carneiro [1], Thomas Mouillot [1,7], Audren Fournel [5], Claude Knauf [5], Christophe Magnan [2], Xavier Fioramonti [1,6], Luc Pénicaud [1], Corinne Leloup [1,*]

ABSTRACT

Objective: Hypothalamic glucose sensing (HGS) initiates insulin secretion (IS) via a vagal control, participating in energy homeostasis. This requires mitochondrial reactive oxygen species (mROS) signaling, dependent on mitochondrial fission, as shown by invalidation of the hypothalamic DRP1 protein. Here, our objectives were to determine whether a model with a HGS defect induced by a short, high fat-high sucrose (HFHS) diet in rats affected the fission machinery and mROS signaling within the mediobasal hypothalamus (MBH).

Methods: Rats fed a HFHS diet for 3 weeks were compared with animals fed a normal chow. Both *in vitro* (calcium imaging) and *in vivo* (vagal nerve activity recordings) experiments to measure the electrical activity of isolated MBH gluco-sensitive neurons in response to increased glucose level were performed. In parallel, insulin secretion to a direct glucose stimulus in isolated islets vs. insulin secretion resulting from brain glucose stimulation was evaluated. Intra-carotid glucose load-induced hypothalamic DRP1 translocation to mitochondria and mROS (H_2O_2) production were assessed in both groups. Finally, compound C was intracerebroventricularly injected to block the proposed AMPK-inhibited DRP1 translocation in the MBH to reverse the phenotype of HFHS fed animals.

Results: Rats fed a HFHS diet displayed a decreased HGS-induced IS. Responses of MBH neurons to glucose exhibited an alteration of their electrical activity, whereas glucose-induced insulin secretion in isolated islets was not affected. These MBH defects correlated with a decreased ROS signaling and glucose-induced translocation of the fission protein DRP1, as the vagal activity was altered. AMPK-induced inhibition of DRP1 translocation increased in this model, but its reversal through the injection of the compound C, an AMPK inhibitor, failed to restore HGS-induced IS.

Conclusions: A hypothalamic alteration of DRP1-induced fission and mROS signaling in response to glucose was observed in HGS-induced IS of rats exposed to a 3 week HFHS diet. Early hypothalamic modifications of the neuronal activity could participate in a primary defect of the control of IS and ultimately, the development of diabetes.

[1]Centre des Sciences du Goût et de l'Alimentation, UMR CNRS 6265, INRA 1324, AgroSup, Univ. Bourgogne Franche-Comté, F-21000 Dijon, France [2]CNRS UMR 8251, Unit of Functional and Adaptive Biology, Paris, France [3]Department of Physiology, Université Paris Diderot, Paris, France [4]STROMALab, UMR CNRS 5273, EFS Pyrénées-Méditerranée, Université Paul Sabatier, Toulouse, France [5]Institut de Recherche en Santé Digestive, INSERM U1220, Université Paul Sabatier, Toulouse, France [6]UMR 1286, NutriNeuro, INRA, Université de Bordeaux, Bordeaux INP, Bordeaux, France [7]Service d'Hépato-Gastroentérologie, hôpital du Bocage, Dijon, France

*Corresponding author. Centre des Sciences du Goût et de l'Alimentation, UMR CNRS 6265, INRA 1324, AgroSup, Université de Bourgogne; 9E boulevard Jeanne d'Arc, F-21000 Dijon, France. Tel.: +33380681665.

E-mails: luciedesmoulins@gmail.com (L. Desmoulins), chloe.chretien21@gmail.com (C. Chrétien), romain.paccoud@hotmail.fr (R. Paccoud), stephan.collins@u-bourgogne.fr (S. Collins), cruciani@univ-paris-diderot.fr (C. Cruciani-Guglielmacci), galinier.a@chu-toulouse.fr (A. Galinier), fabienne.lienard@u-bourgogne.fr (F. Liénard), aurore.quinault@gmail.com (A. Quinault), sylvie.grall@u-bourgogne.fr (S. Grall), camille.allard@gmail.com (C. Allard), claire.fenech@u-bourgogne.fr (C. Fenech), carneiro.lionel@gmail.com (L. Carneiro), thomas.mouillot@gmail.com (T. Mouillot), audren.fournel@gmail.com (A. Fournel), claude.knauf@inserm.fr (C. Knauf), magnan@univ-paris-diderot.fr (C. Magnan), Xavier.fioramonti@inra.fr (X. Fioramonti), luc.penicaud@inserm.fr (L. Pénicaud), corinne.leloup@u-bourgogne.fr (C. Leloup).

Received November 11, 2018 • Revision received November 19, 2018 • Accepted November 22, 2018 • Available online 27 November 2018

https://doi.org/10.1016/j.molmet.2018.11.007

Abbreviations			
aCSF	Artificial cerebrospinal fluid	H$_2$DCFDA	dichlorodihydro-fluorescein diacetate
AMPK	AMP-activated protein kinase	HFHS	High fat-high sucrose diet
ARC	Arcuate nucleus	HGS	Hypothalamic glucose sensing
AUC	Area under the curve	ICV	Intracerebroventricular
Catr	Carboxy-atractyloside	IS	Insulin secretion
CC	Compound C	MBH	Mediobasal hypothalamus
CCCP	Carbonyl cyanide m-chlorophenylhydrazone	MFN (1—2)	Mitochondrial fusion proteins 1 or 2
DRP1	Dynamin-related protein 1	mROS	Mitochondrial reactive oxygen species
FIS1	Fission protein 1	OPA1	Optic atrophy 1
GIIS	Glucose-induced insulin secretion	POMC	Pro-opiomelanocortin
GSH	Reduced form of glutathione	SF1	Steroidogenic factor 1
GSSG	Oxidized form of glutathione	STD	Standard diet
		UCP2	Uncoupling protein 2

1. INTRODUCTION

Obesity and type II diabetes result in dysregulation of energy balance, characterized by increased energy intake and decreased energy expenditure. The hypothalamus and, more particularly, the mediobasal hypothalamus (MBH), which includes the arcuate (ARC) and ventro-medial nuclei, play a central role in maintaining energy homeostasis [1]. The MBH contains neurons that trigger appropriate physiological responses to maintain whole body energy homeostasis in response to blood energy-related stimuli (reviewed in [2,3]). Among these circulating stimuli, glucose activates discrete peripheral responses that are essential for the control of carbohydrate metabolism. For example, increased hypothalamic glucose levels inhibit hepatic glucose production and stimulate glycogen storage [4—6], while stimulating the vagal control of insulin secretion [7—10] and thermogenesis [11—13]. These responses are driven by some hypothalamic neurons sensitive to increases in blood glucose level, at least in the ARC [9,14], although their chemistry remains fundamentally uncertain because only some have been identified.

A transient cerebral hyperglycemia (without affecting peripheral blood glucose level *in vivo*) leads to a rapid peak of insulin secretion (1— 3 min) and contributes to the first phase of glucose-induced insulin secretion (GIIS) ([10] and reviewed by [15,16]). This cascade of events requires the production of mitochondrial reactive oxygen species (mROS), because MBH antioxidants and mitochondrial uncoupling treatments impair both the electrical activation and the insulin peak [9]. Finally, both mROS signaling and increased ARC neuron firing rate in response to cerebral graded doses of glucose are disturbed in models of obesity and insulin resistance [14]. Other studies demonstrated that mROS signaling is essential in some major neuronal ARC populations (reviewed by [17]) which corroborates the crucial role of the relationship between the mitochondrial redox signaling in the ARC and the control of body energy status.

Hypothalamic mROS signaling also requires an upstream event involving mitochondrial dynamics. Continuous cycles of mitochondrial fusion and fission allow mitochondria to bio-energetically adapt to the cellular energy demand and produce adequate signaling [18—20]. In the MBH, we previously showed that increased brain glucose level *in vivo* triggers the translocation of dynamin-related protein 1 (DRP1) to mitochondria, a mechanism required for glucose homeostasis [21]. Since then, other studies have confirmed the role of mitochondrial dynamics in some neuronal populations of the ARC. For example, transgenic mice with a deletion of mitochondrial fusion proteins MFN1 or MFN2 in neurons expressing the Agouti-related protein display

resistance to a diet-induced obesity [22], whereas this deletion in neurons expressing Pro-opiomelanocortin (POMC) induces hypersensitivity to such a diet, because mice rapidly develop hyperphagia, have reduced energy expenditure and become obese [23].

Although it was recently suggested that diet-induced obesity impairs *in vivo* hypothalamic glucose sensing (HGS) [24], the involvement of mitochondrial dynamics and mROS signaling within the MBH has not been studied in this context yet. In this study, we evaluated whether a short period (3 weeks) of high fat-high sucrose diet intake could affect the hypothalamic glucose sensing mechanism compared with rats fed a standard diet and consequently, the *in vivo* HGS-induced insulin secretion (IS). The involvement of hypothalamic DRP1 translocation and mROS signaling in response to brain glucose was investigated to decipher the potential involvement of this pathway in early altered metabolic responses.

2. MATERIALS AND METHODS

2.1. Animals

Male Wistar rats (5 weeks old; Charles River laboratories, Lyon, France) were housed in a controlled environment (12 h light/dark cycle, lights on at 7:00 a.m., 22 ± 1 °C) and fed *ad libitum*. After a week of acclimatization, rats were fed for 3 weeks with a standard diet (STD) (#A04; Safe, Augy, France) or a high fat-high sucrose diet (HFHS) (#HF235; Safe) (see Supplementary Table 1 for diet compositions). Body weight and food intake were recorded daily 3 h after the beginning of the light cycle. Nuclear magnetic resonance was used to determine the body composition of the rats (QNMR system EchoMRI-500T, Echo Medical Systems, Houston, USA). Surgeries and metabolic assessment were performed under anesthesia (sodium pentobarbital 60 mg/kg of body weight; Ceva, Velaine en Haye, France), after a 4 h fasting period. All procedures involving rats were conducted in accordance with the ARRIVE guidelines, European Directive (2010/63/EU) and approved by our local ethic committee of the University of Burgundy (C2EA Grand Campus Dijon N°105) and French Ministry of Research (agreement N° 03035.02).

2.2. Intra-carotid glucose or rotenone injection-induced insulin secretion

Experiments were performed as previously described [9,14]. Briefly, rats were injected over 30 s with a 9 mg/kg glucose load (100 μl) or over 1 min with a 2 μM rotenone load (200 μl) toward the brain through the carotid artery. Blood was collected at the rat tail vein to measure glycemia and insulinemia before and 1, 3, 5 and 10 min after

injection. At the end of the experiment, brains were quickly removed, and the MBH dissected and immediately frozen in liquid nitrogen for further analyses. Plasma and brain samples were stored at $-80\,^{\circ}C$ until assayed.

2.3. Glucose or insulin tolerance test and blood parameter determinations

Rats were either administered glucose (2 g glucose per kg body weight) or insulin (1 U insulin per kg of body weight). Subcutaneous injections were chosen over intraperitoneal route since, in our hands, it presented less variability in blood glucose levels. Blood samples were collected from the tail vein for measurements of blood glucose levels at the indicated times.

Blood glucose concentration was measured using the glucose analyzer Performa AccuChek (Roche Diagnostics, Meylan, France). Plasma insulin and leptin concentrations were determined using ELISA kits according to the manufacturer's recommendations (AlpCo or Biovendor, Eurobio, France).

2.4. Calcium imaging of MBH gluco-excited neurons

Single MBH neurons were prepared from the brain of 8-week-old STD or HFHS diet fed rats and the responses to glucose levels using calcium imaging were recorded as previously described [25].

2.5. Static determination of GIIS from rat islets and insulin content

Isolated islets from HFHS or STD fed rats were assayed in 96-well plates, with 10 islets in suspension per well and 9 to 12 replicates per rat (n = 3 rats per condition). Islets were pre-incubated for 1 h in 250 µl of Krebs-Ringer-HEPES buffer containing in mM: 140 NaCl, 3.6 KCl, 2.6 CaCl$_2$, 0.5 NaH$_2$PO^4, 0.5 MgSO^4.7H$_2$O, 5 HEPES (pH 7.4 with NaOH), 2 NaHCO$_3$ and 2 glucose. The buffer was supplemented with 0.2% bovine serum albumin. Insulin secretion in response to glucose was measured during 1 h static incubations in Krebs-Ringer-HEPES buffer containing 2, 12 or 20 mM glucose. All incubations were conducted at 37 $^{\circ}C$ in humidified 5% CO$_2$ in air. After the 1 h static incubations, the supernatant was removed and stored at $-20\,^{\circ}C$. To determine total insulin content, islets were incubated overnight at $-20\,^{\circ}C$ with acidified ethanol solution (95% ethanol, 5% acetic acid).

2.6. Parasympathetic firing-rate recordings

The firing rate of the thoracic branch of the vagus nerve along the carotid artery was recorded at the end of the experimentation at day 21 as previously described [26]. The vagus nerve of anesthetized rats, which lies close to the carotid artery, was dissected free of underlying tissues to a distance of approximately 1 cm. The nerve was carefully placed on a pair of silver-wire recording electrodes (0.6-mm diameter). The electrodes were connected to a high-impedance probe, and action potentials were displayed and saved on a computer after initial amplification through a low-noise amplifier (BIO amplifier; AD Instrument, Rabalot, France). Rats were first injected with saline through the carotid artery, and, 10 min afterward, they were injected with 9 mg/kg glucose. Unipolar nerve activity was recorded continuously before, during and after both of these injections. Data were digitized with a PowerLab/4sp digitizer. Signals were amplified 105-fold and filtered using low- and high-frequency cut-offs of 1 and 30 Hz, respectively, and monitored using the Chart 4 computer program.

2.7. ROS level measurement

One minute after the beginning of the carotid glucose injection, or five minutes after rotenone injection, rats were decapitated, brains quickly

removed, and the MBH dissected, frozen in liquid nitrogen, and then stored at $-80\,^{\circ}C$. ROS determination was performed as described previously [27] using the fluorescent probe dichlorodihydro-fluorescein diacetate (H$_2$-DCFDA; Molecular Probes, Eugene, OR, USA) that primarily detects H$_2$O$_2$ levels. ROS measurements were performed in a fluorescent plate reader (Perkin Elmer, Courtaboeuf, France) at 535 nm, under excitation at 490 nm. Intensities of fluorescence were calculated as arbitrary units per milligram of protein.

2.8. Determination of hypothalamic glutathione redox state

Anesthetized rats were decapitated, brains quickly removed, and the MBH dissected. Tissue pieces were homogenized in a lysis saline solution (in mM: 3 EDTA, 150 KCl, pH 7.4). Homogenates (50 µl) mixed with 450 µl of 5% metaphosphoric acid were then centrifuged (10,000 g, 10 min, 4 $^{\circ}C$). Final supernatants were used for glutathione assays, performed by reverse-phase high-performance liquid chromatography as previously described [28]. MBH glutathione redox status was calculated as [oxidized form/(oxidized + reduced) forms] per milligram of protein.

2.9. Oxygen consumption measurement on MBH homogenates

Oxygen consumption was measured using a respirometer (Oxygraph-2k; Oroboros Instruments, Innsbruck, Austria). Freshly dissected MBH was homogenized in mitochondrial respiration medium (MiR05) containing saponin for permeabilization. Three milligrams of MBH tissue were transferred into the glass chambers of the respirometer. Mitochondrial state 2 respiration was stimulated by the successive addition of substrates: 10 mM glutamate to stimulate complex I, and 10 mM succinate to stimulate complex II. Then, state 3 respiration was achieved by adding 2.5 mM ADP to measure oxygen consumption when ATP synthesis rate was maximal. Next, 0.75 mM Carboxy-atractyloside (Catr) was added to block ATP synthesis and achieve the state 4 respiration. Finally, to measure the maximal respiration state, 2.5 µM Carbonyl cyanide m-chlorophenylhydrazone (CCCP), a chemical uncoupler, was used. Oxygen consumption was calculated using Data-Graph software. All chemicals were purchased from the Sigma Aldrich Company. Media were prepared according to the guide provided by Oroboros Instruments, with technical sheets available on the company web site at http://www.oroboros.at/.

2.10. Mitochondria isolation of MBH tissue

One minute after the beginning of the carotid glucose injection, rats were decapitated, brains quickly removed, and the MBH dissected and immediately immersed in ice-cold MB + buffer (in mM: 10 HEPES, 210 mannitol, 10 DTT, 70 sucrose, protease inhibitor cocktail [complete EDTA, Roche diagnostics]). Tissue pieces were homogenized with a Dounce homogenizer. Homogenates were centrifuged at 1,000 g for 10 min at 4 $^{\circ}C$, and supernatants were then centrifuged at 10,000 g for 10 min at 4 $^{\circ}C$. Remaining mitochondrial enriched pellet was suspended in MB + buffer and stored at $-80\,^{\circ}C$ until further western blot analysis.

2.11. Western blot analyses

MBH proteins (20 or 40 µg) were separated on 12% SDS-PAGE. Equal number of samples from different groups were loaded on a single gel to quantify differences between groups, control samples representing the 100% reference. No normalization was applied between the different gels since a reference protein was used each time for the quantification. After transfer and blocking, membranes were probed with 1/1,000 mouse anti-OXPHOS (Mitosciences, Euromedex, Mundolsheim, France), 1/10,000 mouse anti-Actin (Millipore, Molsheim,

France), 1/10,000 mouse anti-DRP1 (BD Biosciences, Le Pont-De-Claix, France), 1/500 mouse anti-OPA1 (BD Biosciences), 1/500 rabbit anti-FIS1 (Clinisciences, Montrouge, France), 1/500 mouse anti-MFN2 (Abnova, Montluçon, France), 1/1,000 rabbit anti-phospho AMPK (Cell Signaling, Danvers, MA, USA) and 1/1,000 rabbit anti-AMPK (Cell signaling), 1/1,000 rabbit anti-phospho-DRP1 (Ser616) and anti-phospho-DRP1 (Ser637) (Cell Signaling, Ozyme, France), overnight at 4 °C. Specific bands were detected using a sheep anti-mouse or a donkey anti-rabbit (1/10,000 in TBST-1X) peroxidase-conjugated secondary antibody (GE healthcare, Orsay, France) incubated for 1 h at room temperature. Bands were visualized by chemi-luminescence with the addition of western C reagent (Bio-Rad, Marnes-la-coquette, France) and were exposed to a ChemiDoc XRS + system (BioRad) for densitometry analysis.

2.12. Intraventricular drug injection

Anesthetized rats were implanted with a silastic catheter (VWR, Fontenay-sous-Bois, France) into the right carotid. After vascular surgery, rats were positioned in a stereotaxic device for acute intra-cerebroventricular (ICV, in 3rd ventricle) injection (coordinates: 2.4 mm posterior to bregma, 9 mm below skull). Rats received an ICV injection of an AMPK inhibitor, Compound C (CC; 100 nM in 10 μl; sc-361,173; Santa Cruz, CA, USA) and then received the intra-carotid glucose in-jection as previously described, 60 min after ICV injection. Respective control rats received an ICV vehicle injection (aCSF #3525; TOCRIS, Ellisville, MI, USA). At the end of the experiment, brains were quickly removed, and the MBH dissected and immediately frozen in liquid nitrogen for further western blot analysis. Plasma and brain samples were stored at −80 °C until assayed.

2.13. Statistical analyses

Statistical analyses were performed with GraphPad Prism 6 for Win-dows (GraphPad Software). Data are presented as the mean ± SEM. After testing normality with a Shapiro−Wilk normality test, unpaired t-tests or Mann−Whitney tests were performed. Two-way ANOVAs were followed by a Fisher's LSD post-test, whereas two-way ANOVAs on repeated measures were followed by a Bonferroni post-test to identify significant differences between groups as described in the figure legends. Asterisks (*) or sharp (#) signs indicate significant differences between groups according to the statistical analysis performed: * or # indicates $p < 0.05$; ** or ## indicates $p < 0.01$; *** or ### indicates $p < 0.001$.

3. RESULTS

3.1. A short HFHS diet exposition impaired hypothalamic glucose-induced insulin secretion

Rats fed the HFHS diet exhibited hyperglycemia (STD = 6.3 ± 0.1 vs. HFHS = 7.5 ± 0.1 mM; $p < 0.001$) despite normal plasma insulin levels compared with those of control STD rats (Figure 1A,B). The HFHS rats also had normal daily caloric intake (Figure Supp. 1A) and body weight at the end of the diet (Figure Supp. 1B). Moreover, the study of body composition showed that the hyper-caloric diet induced an in-crease in fat mass (STD = 11.8 ± 0.6 vs. HFHS = $15.1 \pm 0.8\%$ of body weight; $p < 0.05$) counterbalanced by a decrease in lean mass (STD = 76.3 ± 0.5 vs. HFHS = $72.4 \pm 0.5\%$ of body weight; $p < 0.01$) (Figure Supp. 1C). These changes in body composition were associated with an approximate two-fold increase in plasma leptin concentration (STD = 3.0 ± 0.1 vs. HFHS = 5.7 ± 0.4 ng/ml;
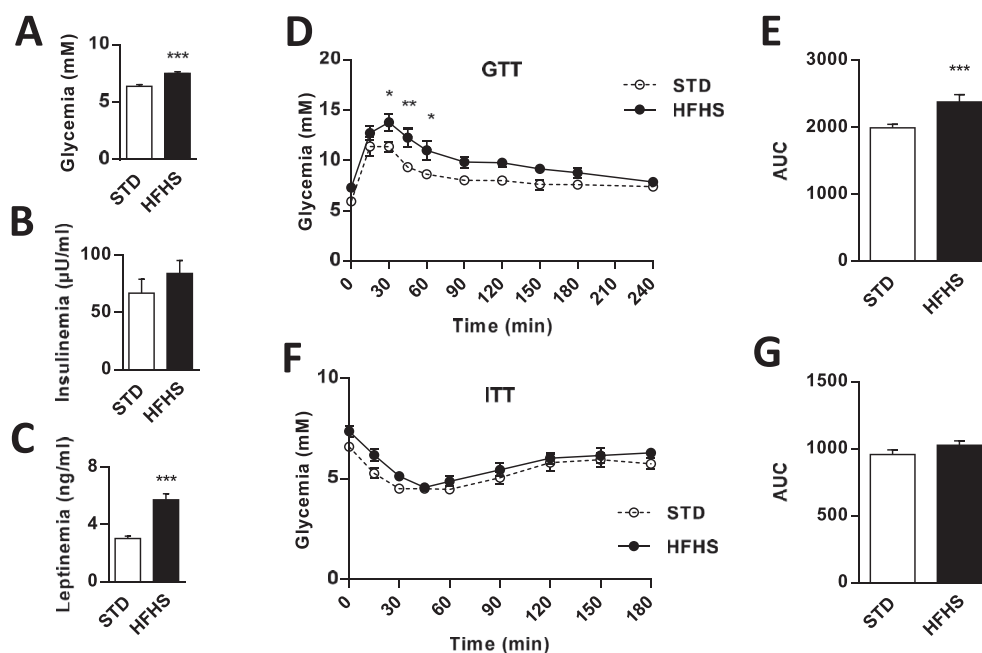

Figure 1: HFHS fed rats exhibit hyperglycemia and glucose intolerance without insulin resistance or significant hyperinsulinemia. (A−B) Basal blood glucose and plasma insulin levels in STD (white bars, n = 15) and HFHS fed rats (black bars, n = 20). **(C)** Plasma leptin level in STD (white bars, n = 41) and HFHS fed rats (black bars, n = 37). **(D−E)** Peripheral blood glucose and AUC in response to a subcutaneous glucose load (2 g/kg of body weight) in STD (dash line, n = 6) and HFHS fed rats (black line, n = 7). **(F−G)** Peripheral blood glucose and AUC in response to a subcutaneous insulin load (1 U/kg of body weight) in STD (dash line, n = 6) and HFHS fed rats (black line, n = 6). Results are expressed as the mean ± SEM; asterisks indicate significant differences between groups according to the statistical analysis performed: *p < 0.05; **p < 0.01; ***p < 0.001.

p < 0.001) (Figure 1C). However, HFHS diet fed rats displayed slight glucose intolerance (AUC in STD = 1993 ± 51 vs. HFHS = 2377 ± 107 mM.s/l; p < 0.001) (Figure 1D,E) without a significant insulin resistance (Figure 1F,G).

HGS-induced IS was secondarily tested in these rats. As previously shown [29], a 30 s glucose load into the carotid artery toward the brain caused a rapid peak of plasma insulin 1 min after the carotid injection in STD rats (T0 min vs. T1 min = +86.1 ± 26.9 µU/ml; p < 0.001), whereas blood glucose levels remained unchanged. However, this peak was not observed in HFHS diet fed rats (T0 min vs. T1 min = +28.9 ± 12.2 µU/ml; p = 0.416; T1 min STD vs. T1 min HFHS: p < 0.05) (Figure 2A,B). This carotid glucose injection also failed to

induce an increase of the vagal tone in HFHS diet fed rats compared with STD fed rats (Figure 2C—E). These data showed that HGS-induced IS was impaired after 3 weeks of HFHS feeding. To confirm this phenotype, we determined whether the response to glucose of MBH neurons was also impaired after HFHS feeding.

Therefore, we performed wide-field single cell imaging of $[Ca^{2+}]_i$ using a Fura-2 calcium probe in freshly dissociated MBH cells in response to an increase in glucose level from 2.5 to 10 mM, as described previously [25]. Whereas the HFHS diet did not alter the number of MBH gluco-excited neurons (STD = 12.5 ± 2.1 vs. HFHS = 12.9 ± 1.9%; p > 0.05); the magnitude of their response to increased glucose concentration decreased dramatically (Figure 2F—H). HFHS feeding did
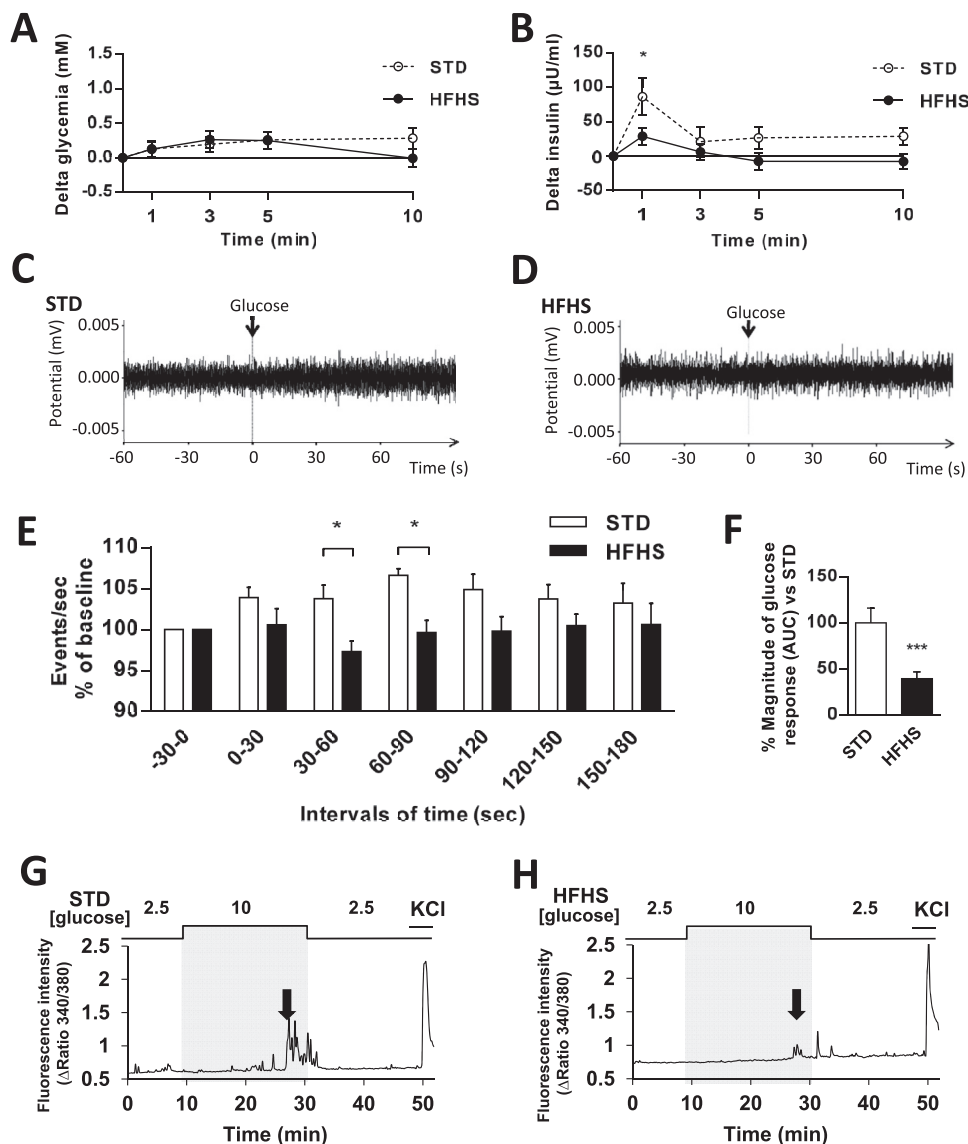

Figure 2: HFHS fed rats display impaired *in vivo* and *in vitro* hypothalamic glucose sensing. (A—B) Blood glucose and plasma insulin levels expressed as delta values (compared with time 0 before injection) in response to an intra-carotid glucose injection (9 mg/kg) in STD (dash line, n = 9) and HFHS fed rats (black line, n = 12). (C—D) Representative recordings of parasympathetic nerve activity from STD (left) and HFHS (right) fed rats 60 s before and 60 s after an intra-carotid glucose injection (9 mg/kg). (E) Parasympathetic nervous system activity recorded in STD (white bars, n = 8) or HFHS fed rats (black bars, n = 7) before and in response to an intra-carotid glucose injection (9 mg/kg) (injection at time 0). (F) Quantification of the magnitude (AUC) of MBH neuron glucose response during calcium imaging study (white bars, STD: n = 31 GE/315 total neurons; black bars, HFHS: n = 34 GE/339 total neurons; 3 independent cultures). (G—H) Representative intracellular calcium traces of MBH GE neuron of STD (left) and HFHS (right) fed rats in response to increased glucose level from 2.5 to 10 mM. Changes in glucose levels are schematically displayed above each recording, and the arrow shows increased intracellular calcium levels. Neuronal excitability was verified at the end of the experiment by addition of KCl. Results are expressed as the mean ± SEM; asterisks indicate significant differences between groups according to the statistical analysis performed: *p < 0.05; ***p < 0.001.

not alter the overall excitability of MBH gluco-excited as determined by their response to 50 mM KCl (response amplitude: STD = 2.3 ± 0.2 vs. HFHS = 1.99 ± 0.3 arbitrary units (Δratio 340/380), p > 0.05). Finally, to verify that the alteration in HGS-induced IS of HFHS diet fed rats was not due to islet dysfunction induced by the short-term hypercaloric diet, GIIS in isolated pancreatic islets was measured. The results showed no significant modification of insulin secretion (Figure 3A) or insulin content after incubation with increased glucose concentration (Figure 3B).

Collectively, these results demonstrated that after only 3 weeks of HFHS feeding, rats displayed a diminished insulin secretion following hypothalamic glucose sensing. This defect was linked to decreased vagal activity, whereas no modification of pancreatic islet sensitivity to glucose occurred.

3.2. Glucose-induced hypothalamic mROS signaling and mitochondrial function are altered in 3 weeks HFHS fed rats

To study whether the alteration in hypothalamic glucose sensing in HFHS fed rats was linked to a defect in mROS signaling, MBH ROS levels were measured 1 min after the intra-carotid injection of saline or glucose, when insulin secretion occurred. As previously shown [9,14,21], the glucose load induced a significant increase in hypothalamic ROS levels in STD fed rats (NaCl vs. Glucose = +33%; p < 0.05). However, this increase did not occur in HFHS diet fed rats (NaCl vs. Glucose = +16%; p = 0.2) (Figure 4A). Notably, in both groups, the basal ROS level assessed after saline intra-carotid injection was similar (STD = 100.0 ± 5.5 vs. HFHS = 91.6 ± 5.1%; p = 0.5) which suggested that the hypothalamic redox state was not affected by the hyper-caloric diet (Figure 4A). To verify this point, the primary cellular antioxidant that reflects the redox state, glutathione, was evaluated. The GSSG (oxidized glutathione) to GSH (reduced form) ratio showed no difference between STD and HFHS diet fed rats (Figure 4B). To verify whether an equivalent MBH ROS production results in a similar peak of insulin between the two groups, we used a specific mitochondrial inhibitor, rotenone, which causes electron blockade that eventually reacts with molecular oxygen, generating superoxide anions at complex I [30]. Injection of rotenone has already been shown to induce ROS production in the hypothalamus as well as IS, thus mimicking the effects of a glucose load [9]. Here, rotenone was able to significantly induce ROS production similarly in STD and HFHS fed rats (STD = 2.45 × 10^6 ± 0.20 × 10^6 vs. HFHS = 2.65 × 10^6 ± 0.22 × 10^6 arbitrary units of fluorescence per mg of protein; p = 0.54) (Figure 5A). This ROS production resulted in an increase in IS (T0 min vs. T1−5 min in STD = +28.87 ± 6.91; p < 0.001 vs. HFHS = +17.48 ± 3.10 μU/ml; p < 0.001) which was

not different between STD and HFHS fed rats (T1−5 min STD vs. T1−5 min HFHS: p = 0.997) (Figure 5B). These results demonstrate that similar ROS production in HFHS fed group compared to control group is sufficient to restore an identical central command inducing IS in HFHS diet fed rats. These results suggest that impaired ROS production in response to glucose, induced by HFHS feeding, contributed in decreased HGS induced IS.

We then explored MBH mitochondrial respiration by oxygraphy. No difference in the basal oxygen consumption between groups occurred (Figure 4C), showing normal mitochondrial respiration in the resting state in the MBH of HFHS fed rats. However, the substrates-driven respiration (state 2 respiration), measured by sequentially adding glutamate to stimulate complex I and succinate to stimulate complex II, revealed a trend toward decreased stimulation with the addition of glutamate (STD = 128.6 ± 3.5 vs. HFHS = 115.6 ± 3.5% of basal oxygen consumption; p = 0.056) and a drastic decrease of the stimulation with the addition of succinate (STD = 400.7 ± 20.8 vs. HFHS = 269.1 ± 10.2% of basal oxygen consumption; p < 0.01) in HFHS compared with STD fed rats. Decreased stimulated oxygen consumption in the MBH of HFHS fed rats remained in state 3 respiration, when adding a saturating concentration of ADP to stimulate complex V (STD = 911.8 ± 41.3 vs. HFHS = 702.6 ± 40.4% of basal oxygen consumption; p < 0.05). However, the inhibition of complex V with Carboxyatractyloside restored a normal respiration in the MBH of HFHS fed rats, showing a normal ADP-independent state 4 respiration (STD = 304.2 ± 25.7 vs. HFHS = 248.2 ± 17.8% of basal oxygen consumption; p = 0.095). This result was confirmed by the respiration rate in the MBH of HFHS fed rats that was not significantly different from STD rats when maximal uncoupled respiration was measured, after CCCP addition (STD = 707.2 ± 42.4 vs. HFHS = 576.9 ± 53.8% of basal oxygen consumption; p = 0.095) (Figure 4D). Thus, these results highlighted a decrease in respiratory chain function coupled to ADP phosphorylation in response to substrates in the MBH of HFHS fed rats, whereas no difference was found regarding these parameters in the cortex (Figure Supp. 2A,B). Moreover, the MBH protein levels of the five mitochondrial complexes were quantified and no difference was found between groups (Figure 4E,F), showing that changes in mitochondrial respiration rates were due to an alteration of mitochondrial complex activity rather than a lower number of complex.

3.3. HFHS fed rats displayed an altered translocation of the fission protein DRP1 to mitochondria in response to glucose within the MBH

We previously highlighted that increased hypothalamic glucose levels trigger the mitochondrial translocation of MBH DRP1, the primary cytoplasmic protein involved in mitochondrial fission [31]. Additionally, inhibiting MBH DRP1 expression blocks mROS production in response to glucose, and ultimately, HGS-induced IS [21].

In that context, we measured the MBH protein levels of the primary players involved in mitochondrial dynamics in rats fed either with STD or HFHS diet. No difference was found in the total protein content of fission proteins 1 (FIS1) (p = 0.912) and DRP1 (p = 0.431) or in fusion proteins MFN2 (p = 0.262) and Optic atrophy 1 (OPA1) (p = 0.696) (Figure 6A,B).

We then further evaluated the mitochondrial MBH DRP1 translocation in response to glucose on mitochondrial fractions extracted from MBH only 1 min after the beginning of the intra-carotid glucose injection. This time corresponded with the peaks of mROS production and insulin secretion. As previously shown [21], the hypothalamic glucose increase induced a significant increase in DRP1 translocation to mitochondria in STD fed rats (NaCl vs. Glucose = +24%, p < 0.05). However, this translocation did not occur in HFHS fed rats (NaCl vs.
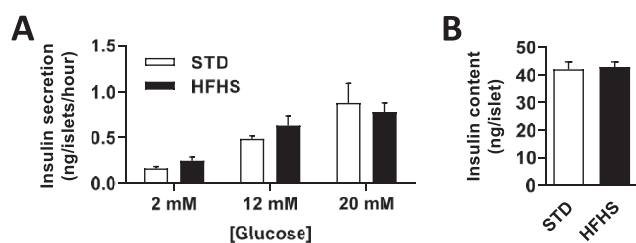
Figure 3: HFHS fed rats have an *ex-vivo* normal GIIS at the islet level. (A) Insulin secretion from STD (white bars, n = 19) or HFHS fed rats (black bars, n = 16) pancreatic islets after increased glucose stimulation (n = 3 rats per condition, 9 to 12 replicates) and **(B)** insulin content in the basal condition. Results are expressed as the mean ± SEM, and no significant difference was found between groups according to the statistical analysis performed.
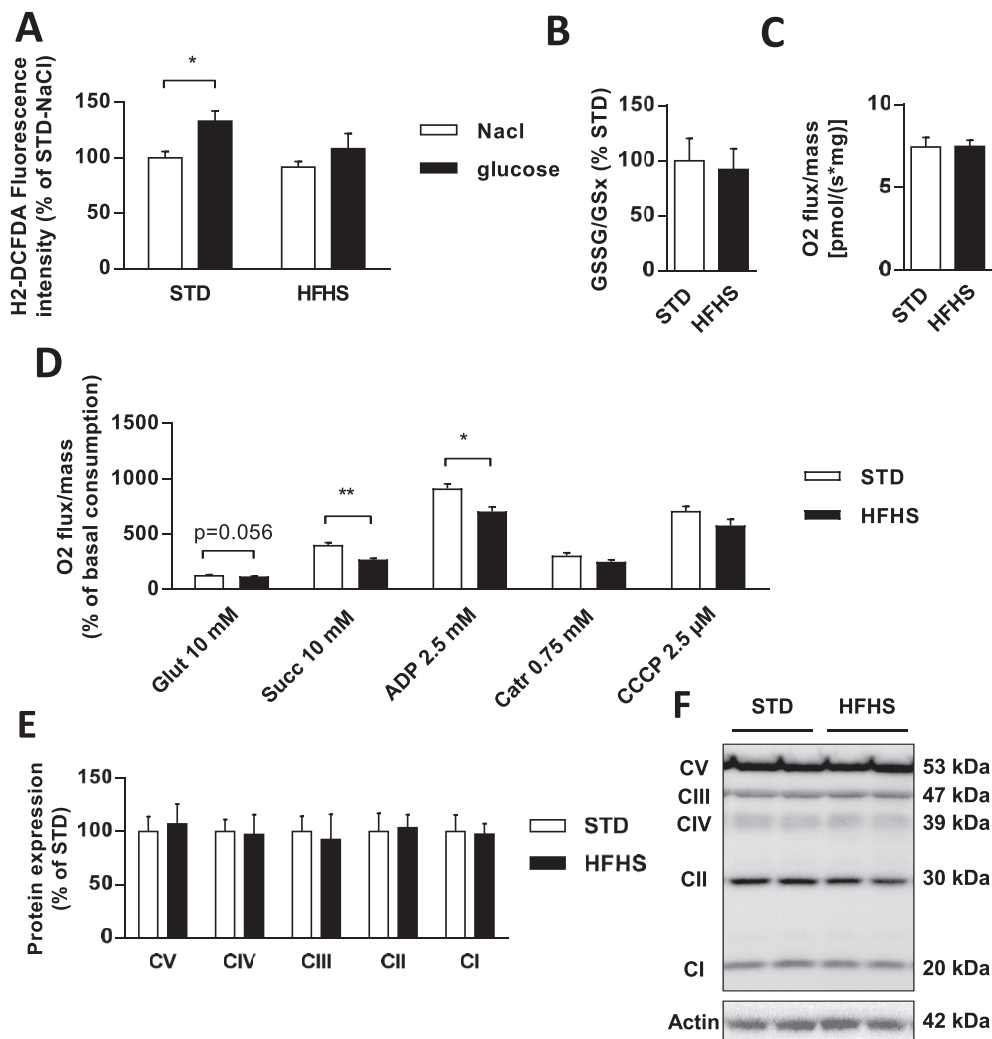
Figure 4: Glucose-induced hypothalamic ROS signaling and mitochondrial respiratory chain function are altered in HFHS fed rats. (A) ROS production in MBH 1 min after an intra-carotid injection of saline (NaCl) or glucose (9 mg/kg) in STD (white bars, n = 10) and HFHS fed rats (black bars, n = 10). Data are expressed in fluorescence related to protein concentration in percentage of STD-NaCl control rats. **(B)** Redox state of glutathione measured by HPLC in hypothalamic homogenates of STD (white bars, n = 7) and HFHS fed rats (black bars, n = 7). **(C−D)** Oxygen consumption measured in MBH during resting state or in response to pharmacological stimulation or inhibition of the different electron transport chain complexes in STD (white bars, n = 5) and HFHS fed rats (black bars, n = 5). Data are expressed in percentage of basal oxygen consumption. **(E−F)** Representative immunoblot and analysis of protein expression of respiratory chain complexes I to V in MBH of STD (white bars, n = 8) and HFHS fed rats (black bars, n = 6). Results are expressed in percentage of STD, after optic density was normalized using the β-actin signal as a reference. Results are expressed as the mean ± SEM; asterisks indicate significant differences between groups according to the statistical analysis performed: *p < 0.05; **p < 0.01.

Glucose = −10%; p = 0.354). Additionally, the mitochondrial DRP1 content after glucose injection was significantly lower in the MBH of HFHS diet fed rats than in that of STD fed rats (STD = 123.6 ± 7.5 vs. HFHS = 86.1 ± 6.9%; p < 0.01) (Figure 6C,D).
DRP1 translocation to the mitochondria involves several post-translational modifications of the protein, such as sumoylation, S-nitrosylation, ubiquitination, and phosphorylation [32]. However, the ratio between phosphorylated DRP1 and DRP1 is usually used as a readout of DRP1 activity [33]. Thus, we measured the phosphorylation levels of DRP1, both the pro-fission site Ser616 and the anti-fission site Ser637 in MBH extracted 1 min after the beginning of the intra-carotid glucose injection. Surprisingly, no significant difference in the phosphorylation level of the pro-fission site (p = 0.779) or of the anti-fission site (p = 0.354) was present between STD and HFHS fed rats (Figure 6E,F).

Altogether, our data highlighted that 3 weeks of HFHS feeding impaired mitochondrial dynamics in the MBH in response to glucose and more particularly, the fission machinery through the mitochondrial DRP1 translocation process. However, these results also suggested that phosphorylation is not the trigger for DRP1 translocation to mito-chondria in response to glucose in our model.

3.4. Increased AMPK activation is not responsible for altered hypothalamic glucose sensing in 3 weeks HFHS diet fed rats
We finally aimed at restoring DRP1 translocation to mitochondria in the hypothalamus of HFHS fed rats to see if it could restore HGS induced IS. From our current knowledge, it is not possible to specifically ex-press an active form of DRP1 and overexpressing DRP1 would not be relevant as its total expression was not affected in HFHS fed rats. However, it is possible to modulate the activity of factors such as AMP-
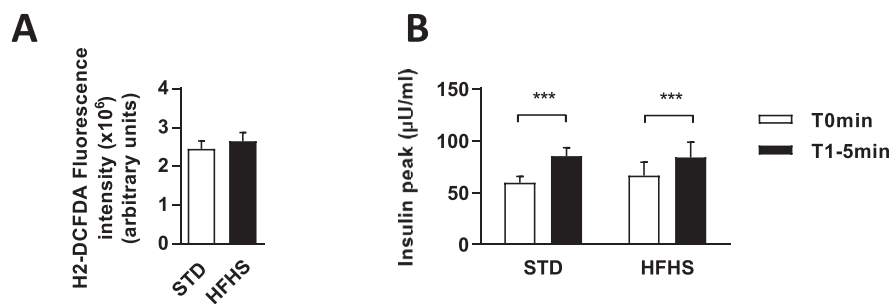
Figure 5: Rotenone-induced hypothalamic ROS production and insulin secretion similarly in STD and HFHS fed rats. **(A)** ROS production in MBH 5 min after an intra-carotid injection of rotenone in STD (white bar, n = 6) and HFHS fed rats (black bar, n = 9). Data are expressed in arbitrary units of fluorescence related to protein concentration. **(B)** Plasma insulin levels in response to an intra-carotid injection of rotenone in STD (n = 6) and HFHS fed rats (n = 9), before injection (white bars, T0 min) and when peak of insulin occurs at 1, 3 or 5 min after intra-carotid injection (black bars, T1−5 min). Results are expressed as the mean ± SEM; asterisks indicate significant differences between, before and after injection among groups according to the statistical analysis performed: ***$p < 0.001$.
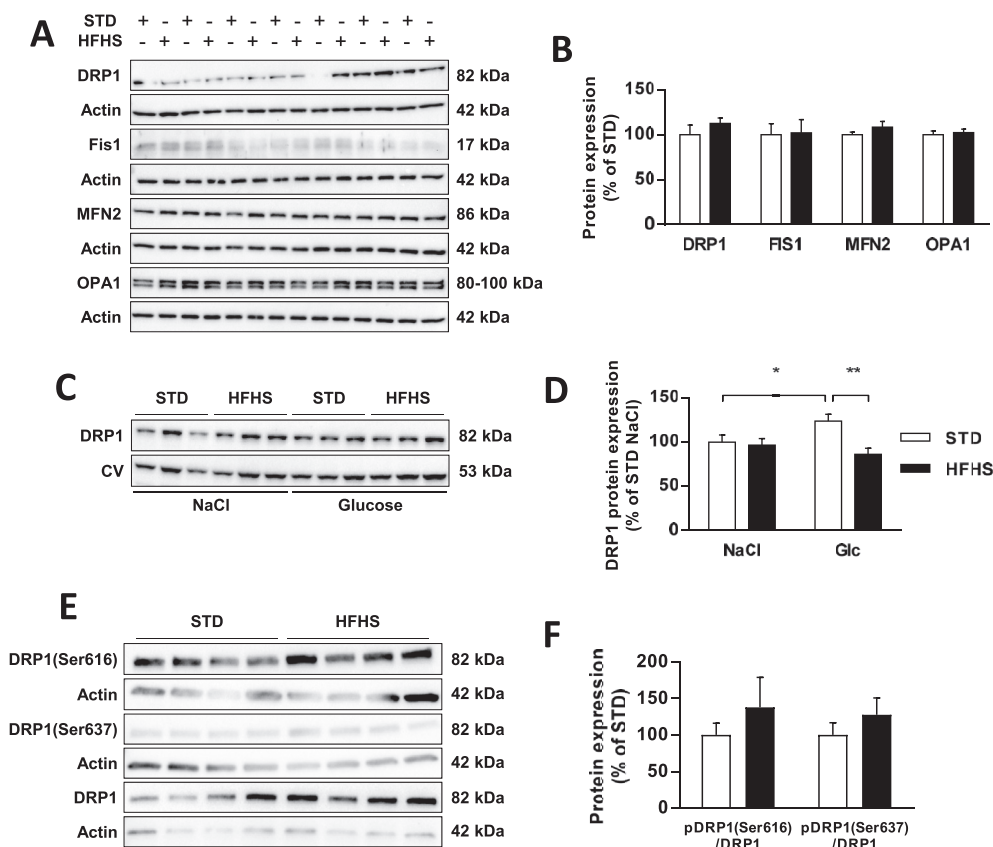

Figure 6: Glucose-induced mitochondrial fission is altered in HFHS fed rats. **(A)** Representative immunoblots and **(B)** analysis of protein expression involved in mitochondrial dynamics during resting state in STD (white bars, n = 7) and HFHS fed rats (black bars, n = 7). DRP1 and FIS1 correspond to fission proteins, whereas MFN2 and OPA1 correspond to fusion proteins. Results are expressed in percentage of STD, after optic density was normalized using the β-actin signal as a reference. **(C)** Representative immunoblots and **(D)** analysis of DRP1 translocation to mitochondria after an intra-carotid injection of saline (NaCl) or glucose (9 mg/kg) in STD (white bars, n = 6) and HFHS fed rats (black bars, n = 6). Results are expressed in percentage of STD-NaCl, after optic density was normalized using the Complex V signal (55 kDa) as a reference. **(E)** Representative immunoblots and **(F)** analysis of phosphorylation levels of DRP1 on MBH extracted 1 min after the beginning of an intra-carotid injection of glucose (9 mg/kg) in STD (white bars, n = 8) and HFHS fed rats (black bars, n = 8). Results are expressed in as a ratio between pDRP1 and DRP1 in percentage of STD, after optic density was normalized using actin signal (42 kDa) as a reference. **(E)** Results are expressed as the mean ± SEM; asterisks indicate significant differences between groups according to the statistical analysis performed: *$p < 0.05$; **$p < 0.01$.

activated protein kinase (AMPK), a nutrient sensor known as a key regulator of mitochondrial fission [34,35]. In that context, we speculated that AMPK might be abnormally active in the MBH of HFHS fed rats as previously described [36—38]. Thus, inhibiting AMPK activity would increase DRP1 translocation to the mitochondria and improve glucose sensing in the MBH of HFHS fed rats. Whereas our results showed that HFHS diet fed rats did have a significant increase in pAMPK/AMPK ratio in the MBH (STD vs. HFHS = +120%; $p < 0.001$) (Figure 7A,B), the rescue of the MBH pAMPK/AMPK ratio, through compound C treatment by ICV injection (HFHS-aCSF = 220.9 ± 17.3 vs. HFHS-CC = $134.7 \pm 7.6\%$; $p < 0.001$; STD-aCSF vs. HFHS-CC: $p = 0.112$) (Figure 7A,B), was inefficient to restore, even partially, HGS-induced IS in these rats (plasma insulin 1 min after intra-carotid glucose injection: STD-aCSF = 64.7 ± 7.7 vs. HFHS-CC = 16.0 ± 15.1 μU/ml; $p < 0.01$) (Figure 7C). Thus, these results suggested that decreasing AMPK activity in HFHS fed rats, did not improve HGS-induced IS.

4. DISCUSSION

To study the importance of aspects of brain mitochondrial dynamics in diet-induced early metabolic defects, we first generated a model of early hypothalamic dysregulation to nutrient sensitivity; animals fed 3 weeks an HFHS diet developed an absence of response to brain hyperglycemia in terms of insulin secretion. Both hypothalamic neuron responses to glucose, in vitro, and the vagal activity, in vivo, were disturbed, whereas the direct response of the β cells to glucose was preserved. The hypothalamic impairment was concomitant with decreased mROS signaling and an abnormal mitochondrial respiration. These features were associated with a disruption of the capability of the fission protein DRP1 to translocate to mitochondria in response to brain hyperglycemia within the MBH, an essential process involved in mitochondrial fission. Notably, despite a dysregulated MBH AMPK pathway, previously described as involved in inhibiting the fission machinery [34,35], the restoration of this pathway did not rescue HGS-induced IS in HFHS fed rats.

An HFHS diet supply was chosen to mimic bad eating habits in metabolic disorders in humans such as obesity and type II diabetes in a rodent [39]. Feeding on this diet for only three weeks was too short to induce an overweight phenotype in these rats, because they showed no modification of their energy intake and body weight, despite an increase in fat mass counterbalanced by a decrease in lean mass. This change in body composition was correlated with increased blood glucose and triglycerides and a twofold increase in leptin level with no significant modification of plasma insulin. Additionally, this HFHS diet fed rat model displayed slight glucose intolerance with no sign of insulin resistance. Altogether, these data suggest that to study early stages of type II diabetes, these animals provide an interesting model. The prerequisite of our model was the alteration of brain glucose sensing, which was first demonstrated by the absence of insulin secretion after a carotid glucose injection toward the brain. Such a glucose load induces a transient insulin secretion controlled by the parasympathetic nervous system and originating from the ARC [7,9]. However, HFHS feeding might also alter islet function, which could have been responsible for the absence of insulin secretion in response to brain glucose [40]. Moreover, increased leptin level is thought to exert an inhibitory effect on insulin secretion [41], an effect that has been recently challenged [42]. We excluded those hypotheses because in vitro pancreatic islets had normal insulin content and could continue to secrete insulin in response to glucose, in a dose-dependent manner, showing intact islet responsiveness. Finally, the hypothalamic origin was confirmed by the following: 1) calcium imaging on freshly dissociated hypothalamic neurons from HFHS fed rats that displayed a decreased response to glucose in vitro; and 2) decreased vagal activity in these animals. Collectively, these data highlight an interesting feature of this model, that is, an early alteration of brain sensitivity to glucose, whereas no abnormal GIIS was observed in isolated islets. These results are consistent with those of previous studies suggesting an autonomous defect that has its origin at the hypothalamic level and that might be one of the primary regulators disturbed in malnutrition models [10,43].

We previously demonstrated that increased electrical activity in ARC neurons in response to a glucose challenge, in vivo, requires a redox signaling, through H_2O_2 production [9]. This H_2O_2 signaling originates from the mitochondrial anion superoxide production and is required to activate gluco-sensitive neurons, with a disturbed activity in installed obese, insulin-resistant animals combined with altered antioxidant activities [14]. In this model, increased mROS signaling in response to a brief brain hyperglycemia was no longer observed in HFHS fed animals after only three weeks. Moreover, basal levels of ROS were identical in STD and HFHS fed rats, and no modification of red/ox glutathione levels, a representation of the cellular redox state, occurred. This result highlighted that the primary defect concerned mitochondrial functioning rather than a decline in antioxidant defenses. Additionally, restoring an identical mROS production by an intra-carotid injection of rotenone was able to induce IS in both STD and HFHS fed
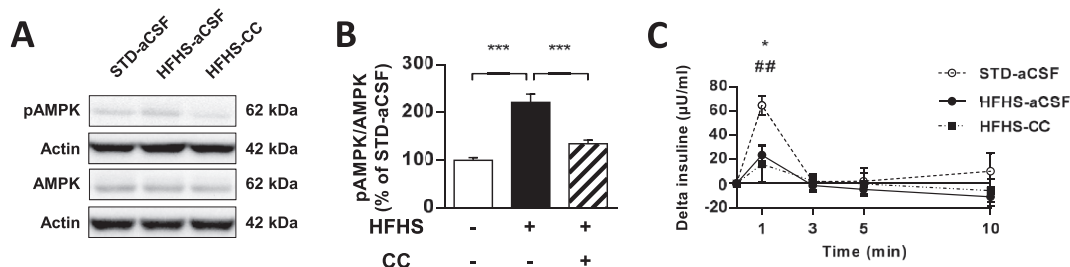

Figure 7: Increased AMPK activation is not responsible for altered hypothalamic glucose sensing in HFHS fed rats. (A) Representative immunoblots and **(B)** analysis of pAMPK/AMPK ratio in MBH of STD fed rats injected with aCSF (white bars, n = 7), HFHS fed rats injected with aCSF (black bars, n = 6) and HFHS fed rats injected with AMPK inhibitor CC (striped bars, n = 6). **(C)** Plasma insulin secretion expressed in delta from basal in response to an intra-carotid glucose injection (9 mg/kg) in STD fed rats injected with aCSF (dash line, n = 6), HFHS fed rats injected with aCSF (black line, n = 6) and HFHS fed rats injected with AMPK inhibitor CC (dotted line, n = 7). Results are expressed as the mean ± SEM; asterisks indicate significant difference between STD-aCSF and HFHS-aCSF or between HFHS-aCSF and HFHS-CC, and a sharp sign indicates significant difference between STD-aCSF and HFHS-CC, according to the statistical analysis performed (*$p < 0.05$; ***$p < 0.001$; ##$p < 0.01$).

rats. Thus, bypassing the mitochondrial DRP1 translocation in response to glucose (as suggested in this hypothesis) led to a peak of insulin that was similar between the two groups. This important result suggests that steps downstream of ROS production, i.e., ROS signaling and redox targets, were not affected in the HFHS group after 3 weeks on this diet.

Because the redox signaling originates in mitochondria and, more particularly, in the electron transport chain, mitochondrial respiration was explored. Mitochondrial O_2 consumption decreased in response to complex II and complex V stimulation. Their roles are to oxidize $FADH_2$ and to dissipate the increased H^+ gradient to generate ATP, when required, respectively. No modification of the protein levels was observed for all five complexes, and decoupling the respiration with CCCP revealed no difference of maximal respiration. These data indicated mostly a decreased acceleration of OXPHOS, i.e., coupled respiration, due to decreased activity of complexes II and V. This reduced activity secondarily imposes a deceleration of electron transport rates and might account for the decreased mROS signaling observed in the MBH of HFHS fed animals, with this signaling directly correlated with the probability of increased electrons to reduce O_2.

Mitochondrial complex activity and respiration are related to mitochondrial dynamics. Our previous work demonstrated that the translocation of the mitochondrial fission protein DRP1 in response to glucose is required to generate the hypothalamic mROS production [21]. Here, brain hyperglycemia-induced DRP1 translocation to mitochondria no longer occurred in HFHS fed rats, suggesting that decreased mitochondrial fission could affect mitochondrial complex organization and function and ultimately, mROS signaling. The relationship between DRP1 translocation to mitochondria and ROS production in response to a glucose load has been recently studied in the hypothalamus. Indeed, neurons expressing the Steroidogenic factor 1 (SF1), located in the ventromedial hypothalamus (which is close to the ARC), showed an increase in mitochondrial fission but a decrease in ROS production in response to a glucose load that was under the control of the uncoupling protein UCP2 [33]. Transgenic mice exhibiting a deletion of UCP2 in SF1 neurons had no increase in phosphorylated DRP1 in response to glucose, and therefore, no further translocation of the protein to mitochondria and consequent fission. By contrast, selective re-expression of UCP2 in these neurons restored the phosphorylation of DRP1. Conversely, POMC neurons with a deletion of DRP1 resulted in improved glucose responsiveness [44].

These discrepancies are related to the models in which a constitutive deletion of DRP1 targeted a single neuronal population, whereas, in our case, all hypothalamic cells were of concern, including neurons sensitive to hyperglycemia (either excited or inhibited) and non-neuronal cells. The latter represent the majority of brain cells, especially astrocytes whose responses to a chronic high caloric diet has suggested an important role in the regulation of energy homeostasis [45,46]. Of the numerous roles identified in glial cells, those related to energy demands are particularly important [47] and might be of particular concern in this acute response to glucose.

While discriminating the role of DRP1 between neuronal and non-neuronal cells was not feasible in this *in vivo* study, there is evidence that mitochondrial DRP1-dependent fission in non-neuronal cells is at least as important as in neurons. Notably, recent works have identified that mitochondria are present in astrocytic processes or in myelin sheaths [48], compartments that were previously thought to be too small to accommodate these organelles [49—51], completely modifying our mindset of how energy is processed into these sites. In neurons, DRP1 mediated mitochondrial fission allows these organelles

to have access to spines and filopodia, while DRP1-induced fission inhibition reduces the number of mitochondria that are present in dendrites and synaptic terminals (reviewed in [52]).

In this study, the disruption of DRP1 translocation to subcellular compartments might affect both glial and neuronal cells that possess diverse mitochondrial number and morphology, and that the dominant mechanism in the MBH is mitochondrial fission increasing mitochondrial ROS in response to glucose.

DRP1 translocation is a complex event, involving multiple post-translational modifications [32]. Indeed, DRP1 must be phosphorylated in its pro-fission site Ser616 to induce mitochondrial fission. Consequently, there are two well established methods for measuring DRP1 translocation to the mitochondria: 1) quantifying total DRP1 in cellular fraction which does not contain the cytoplasm [34,53—55], or 2) quantifying the phosphorylated state of DRP1 on total lysate [34,56,57]. Our results showed that DRP1 translocation is altered in HFHS fed rats in response to glucose using the first method; however, by quantifying the different phosphorylation state of DRP1, we could not find any difference between STD and HFHS fed rats. These results suggest that the phosphorylation of DRP1 was not altered or other post-translational modifications might have contributed to the defect. Recent studies described that the phosphorylation of DRP1 can be dependent on AMPK activation, because pharmacological activation of AMPK increased the phosphorylation of the anti-fission site Ser637, preventing mitochondrial fission [34,35]. In our study, AMPK activation within the MBH increased in HFHS fed rats, suggesting AMPK should have prevented DRP1 translocation. However, the inhibition of AMPK activation by an ICV treatment with compound C did not restore, at least partially, HGS-induced IS. This result suggested AMPK activation inhibited fission might not be involved in this phenotype or might not be the sole factor implicated.

5. CONCLUSION

This study shows for the first time that glucose-induced DRP1 translocation to mitochondria and ROS production in the MBH is compromised in rats fed an HFHS diet for a short period of time (3 weeks), whereas the upstream signals remains undetermined. These findings are consistent with those in our previous study in which DRP1 inhibition prevented normal HGS-induced IS and more recently, with the importance of DRP1 highlighted in SF1 or POMC neurons in response to glucose [21,33,44]. HGS-induced IS is an important part of the control of whole-body metabolism and food intake, which is apparently altered before pancreatic GIIS in β cells in our model and without modification in food intake or body weight but with early disturbances of glucose metabolism. Alteration of HGS-induced IS might be an early event in type II diabetes development, and the reversal of this phenotype, focusing on glucose-induced DRP1 translocation, could be a challenging but important element for further experiments into dealing with the pathogenesis of diabetes.

Original Article

CONFLICTS OF INTEREST

None.

APPENDIX A.   SUPPLEMENTARY DATA

Supplementary data to this article can be found online at https://doi.org/10.1016/j.molmet.2018.11.007.

REFERENCES

[1] Abizaid, A., Horvath, T.L., 2008. Brain circuits regulating energy homeostasis. Regulatory Peptides 149(1–3):3–10. https://doi.org/10.1016/j.regpep.2007.10.006.

[2] Blouet, C., Schwartz, G.J., 2010. Hypothalamic nutrient sensing in the control of energy homeostasis. Behavioural Brain Research 209(1):1–12. https://doi.org/10.1016/j.bbr.2009.12.024.

[3] Schneeberger, M., Gomis, R., Claret, M., 2014. Hypothalamic and brainstem neuronal circuits controlling homeostatic energy balance. The Journal of Endocrinology 220(2):T25–T46. https://doi.org/10.1530/JOE-13-0398.

[4] Lam, T.K., Gutierrez-Juarez, R., Pocai, A., Rossetti, L., 2005. Regulation of blood glucose by hypothalamic pyruvate metabolism. Science (New York, N.Y.) 309(5736):943–947. https://doi.org/10.1126/science.1112085.

[5] Pocai, A., Lam, T.K.T., Gutierrez-Juarez, R., Obici, S., Schwartz, G.J., Bryan, J., et al., 2005. Hypothalamic K(ATP) channels control hepatic glucose production. Nature 434(7036):1026–1031. https://doi.org/10.1038/nature03439.

[6] Yang, C.S., Lam, C.K.L., Chari, M., Cheung, G.W.C., Kokorovic, A., Gao, S., et al., 2010. Hypothalamic AMP-activated protein kinase regulates glucose production. Diabetes 59(10):2435–2443. https://doi.org/10.2337/db10-0221.

[7] Niijima, A., 1975. The effect of glucose on the activity of the adrenal nerve and pancreatic branch of the vagus nerve in the rabbit. Neuroscience Letters 1(3):159–162.

[8] Atef, N., Laury, M.C., N'Guyen, J.M., Mokhtar, N., Ktorza, a., Penicaud, L., 1997. Increased pancreatic islet blood flow in 48-hour glucose-infused rats: involvement of central and autonomic nervous systems. Endocrinology 138(5):1836–1840. https://doi.org/10.1210/endo.138.5.5094.

[9] Leloup, C., Magnan, C., Benani, A., Bonnet, E., Alquier, T., Offer, G., et al., 2006. Mitochondrial reactive oxygen species are required for hypothalamic glucose sensing. Diabetes 55(7):2084–2090. https://doi.org/10.2337/db06-0086.

[10] Osundiji, M. a., Lam, D.D., Shaw, J., Yueh, C.-Y., Markkula, S.P., Hurst, P., et al., 2012. Brain glucose sensors play a significant role in the regulation of pancreatic glucose-stimulated insulin secretion. Diabetes 61(2):321–328. https://doi.org/10.2337/db11-1050.

[11] Le Feuvre, R.A., Woods, A.J., Stock, M.J., Rothwell, N.J., 1991. Effects of central injection of glucose on thermogenesis in normal, VMH- lesioned and genetically obese rats. Brain Research 547(1):110–114.

[12] Voss-Andreae, A., Murphy, J.G., Ellacott, K.L.J., Stuart, R.C., Nillni, E.A., Cone, R.D., et al., 2007. Role of the central melanocortin circuitry in adaptive thermogenesis of brown adipose tissue. Endocrinology 148(4):1550–1560. https://doi.org/10.1210/en.2006-1389.

[13] Berglund, E.D., Liu, T., Kong, X., Sohn, J.-W., Vong, L., Deng, Z., et al., 2014. Melanocortin 4 receptors in autonomic neurons regulate thermogenesis and glycemia. Nature Neuroscience(June):1–4. https://doi.org/10.1038/nn.3737.

[14] Colombani, A., Carneiro, L., Benani, A., Galinier, A., Jaillard, T., Duparc, T., et al., 2009. Enhanced hypothalamic glucose sensing in obesity: alteration of redox signaling. Diabetes 58(10):2189–2197. https://doi.org/10.2337/db09-0110.

[15] Niijima, A., 1989. Neural mechanisms in the control of blood glucose concentration. The Journal of Nutrition 119(6):833–840.

[16] Pénicaud, L., Leloup, C., Fioramonti, X., Lorsignol, A., Benani, A., 2006. Brain glucose sensing: a subtle mechanism. Current Opinion in Clinical Nutrition and Metabolic Care 9(4):458–462. https://doi.org/10.1097/01.mco.0000232908.84483.e0.

[17] Horvath, T.L., Andrews, Z.B., Diano, S., 2009. Fuel utilization by hypothalamic neurons: roles for ROS. Trends in Endocrinology and Metabolism: TEM 20(2):78–87. https://doi.org/10.1016/j.tem.2008.10.003.

[18] Liesa, M., Shirihai, O.S., 2013. Mitochondrial dynamics in the regulation of nutrient utilization and energy expenditure. Cell Metabolism 17(4):491–506. https://doi.org/10.1016/j.cmet.2013.03.002.

[19] Nasrallah, C.M., Horvath, T.L., 2014. Mitochondrial dynamics in the central regulation of metabolism. Nature Reviews Endocrinology 10(11):650–658. https://doi.org/10.1038/nrendo.2014.160.

[20] Putti, R., Sica, R., Migliaccio, V., Lionetti, L., 2015. Diet impact on mitochondrial bioenergetics and dynamics. Frontiers in Physiology 6(April):1–7. https://doi.org/10.3389/fphys.2015.00109.

[21] Carneiro, L., Allard, C., Guissard, C., Fioramonti, X., Tourrel-Cuzin, C., Bailbé, D., et al., 2012. Importance of mitochondrial dynamin-related protein 1 in hypothalamic glucose sensitivity in rats. Antioxidants and Redox Signaling 17(3):433–444. https://doi.org/10.1089/ars.2011.4254.

[22] Dietrich, M.O., Liu, Z.-W., Horvath, T.L., 2013. Mitochondrial dynamics controlled by mitofusins regulate agrp neuronal activity and diet-induced obesity. Cell 155(1):188–199. https://doi.org/10.1016/j.cell.2013.09.004.

[23] Schneeberger, M., Dietrich, M.O., Sebastián, D., Imbernón, M., Castaño, C., Garcia, A., et al., 2013. Mitofusin 2 in POMC neurons connects ER Stress with Leptin resistance and energy imbalance. Cell 155(1):172–187. https://doi.org/10.1016/j.cell.2013.09.003.

[24] de Andrade, I.S., Zemdegs, J.C.S., de Souza, A.P., Watanabe, R.L.H., Telles, M.M., Nascimento, C.M.O., et al., 2015. Diet-induced obesity impairs hypothalamic glucose sensing but not glucose hypothalamic extracellular levels, as measured by microdialysis. Nutrition & Diabetes 5(6):e162. https://doi.org/10.1038/nutd.2015.12.

[25] Chrétien, C., Fenech, C., Liénard, F., Grall, S., Chevalier, C., Chaudy, S., et al., 2017. Transient Receptor Potential Canonical 3 (TRPC3) channels are required for hypothalamic glucose detection and energy homeostasis. Diabetes 66(2):314–324. https://doi.org/10.2337/db16-1114.

[26] Magnan, C., Collins, S., Berthault, M.F., Kassis, N., Vincent, M., Gilbert, M., et al., 1999. Lipid infusion lowers sympathetic nervous activity and leads to increased beta-cell responsiveness to glucose. The Journal of Clinical Investigation 103(3):413–419. https://doi.org/10.1172/JCI3883.

[27] Szabados, E., Fischer, G.M., Toth, K., Csete, B., Nemeti, B., Trombitas, K., et al., 1999. Role of reactive oxygen species and poly-ADP-ribose polymerase in the development of AZT-induced cardiomyopathy in rat. Free Radical Biology & Medicine 26(3–4):309–317.

[28] Galinier, A., Carrière, A., Fernandez, Y., Carpéné, C., André, M., Caspar-Bauguil, S., et al., 2006. Adipose tissue proadipogenic redox changes in obesity. The Journal of Biological Chemistry 281(18):12682–12687. https://doi.org/10.1074/jbc.M506949200.

[29] Leloup, C., Orosco, M., Serradas, P., Nicolaïdis, S., Pénicaud, L., 1998. Specific inhibition of GLUT2 in arcuate nucleus by antisense oligonucleotides suppresses nervous control of insulin secretion. Brain Research. Molecular Brain Research 57(2):275–280.

[30] Turrens, J.F., 1997. Superoxide production by the mitochondrial respiratory chain. Bioscience Reports 17(1):3–8.

[31] Smirnova, E., Griparic, L., Shurland, D.L., van der Bliek, A.M., 2001. Dynamin-related protein Drp1 is required for mitochondrial division in mammalian cells. Molecular Biology of the Cell 12(8):2245–2256.

[32] Archer, S.L., 2013. Mitochondrial dynamics–mitochondrial fission and fusion in human diseases. The New England Journal of Medicine 369(23):2236–2251. https://doi.org/10.1056/NEJMra1215233.

[33] Toda, C., Kim, J.D., Impellizzeri, D., Cuzzocrea, S., Liu, Z.-W., Diano, S., 2016. UCP2 regulates mitochondrial fission and ventromedial nucleus control of glucose responsiveness. Cell 164(5):872–883. https://doi.org/10.1016/j.cell.2016.02.010.

[34] Wikstrom, J.D., Israeli, T., Bachar-Wikstrom, E., Swisa, A., Ariav, Y., Waiss, M., et al., 2013. AMPK regulates ER morphology and function in stressed pancreatic β-cells via phosphorylation of DRP1. Molecular Endocrinology (Baltimore, Md.) 27(10):1706–1723. https://doi.org/10.1210/me.2013-1109.

[35] Toyama, E.Q., Herzig, S., Courchet, J., Jr, T.L.L., Oliver, C., Hellberg, K., et al., 2016. Response To Energy Stress 351(6270):275–281. https://doi.org/10.1126/science.aab4138.AMP-activated.

[36] Cavaliere, G., Viggiano, E., Trinchese, G., De Filippo, C., Messina, A., Monda, V., et al., 2018. Long feeding high-fat diet induces hypothalamic oxidative stress and inflammation, and prolonged hypothalamic AMPK activation in rat animal model. Frontiers in Physiology 9:818. https://doi.org/10.3389/fphys.2018.00818.

[37] Carneiro, L., Geller, S., Fioramonti, X., Hébert, A., Repond, C., Leloup, C., et al., 2016. Evidence for hypothalamic ketone body sensing: impact on food intake and peripheral metabolic responses in mice. American Journal of Physiology. Endocrinology and Metabolism 310(2):E103–E115. https://doi.org/10.1152/ajpendo.00282.2015.

[38] Viggiano, E., Mollica, M.P., Lionetti, L., Cavaliere, G., Trinchese, G., De Filippo, C., et al., 2016. Effects of an high-fat diet enriched in lard or in fish oil on the hypothalamic amp-activated protein kinase and inflammatory mediators. Frontiers in Cellular Neuroscience 10:150. https://doi.org/10.3389/fncel.2016.00150.

[39] Gerbaix, M., Metz, L., Mac-Way, F., Lavet, C., Guillet, C., Walrand, S., et al., 2012. Impact of an obesogenic diet program on bone densitometry, micro architecture and metabolism in male rat. Lipids in Health and Disease 11(1):91. https://doi.org/10.1186/1476-511X-11-91.

[40] Talchai, C., Lin, H.V., Kitamura, T., Accili, D., 2009. Genetic and biochemical pathways of β-cell failure in type 2 diabetes. Diabetes, Obesity and Metabolism 11:38–45. https://doi.org/10.1111/j.1463-1326.2009.01115.x.

[41] Kieffer, T.J., Habener, J.F., 2000. The adipoinsular axis: effects of leptin on pancreatic beta-cells. American Journal of Physiology. Endocrinology and Metabolism 278(1):E1–E14.

[42] Soedling, H., Hodson, D.J., Adrianssens, A.E., Gribble, F.M., Reimann, F., Trapp, S., et al., 2015. Limited impact on glucose homeostasis of leptin receptor deletion from insulin- or proglucagon-expressing cells. Molecular Metabolism 4(9):619–630. https://doi.org/10.1016/j.molmet.2015.06.007.

[43] Cruciani-Guglielmacci, C., Vincent-Lamon, M., Rouch, C., Orosco, M., Ktorza, A., Magnan, C., 2005. Early changes in insulin secretion and action induced by high-fat diet are related to a decreased sympathetic tone. American Journal of Physiology. Endocrinology and Metabolism 288(1):E148–E154. https://doi.org/10.1152/ajpendo.00225.2004.

[44] Santoro, A., Campolo, M., Liu, C., Sesaki, H., Meli, R., Liu, Z.-W., et al., 2017. DRP1 suppresses leptin and glucose sensing of POMC neurons. Cell Metabolism, 1–14. https://doi.org/10.1016/j.cmet.2017.01.003.

[45] Wang, Y., Hsuchou, H., He, Y., Kastin, A.J., Pan, W., 2015. Role of astrocytes in leptin signaling. Journal of Molecular Neuroscience 56(4):829–839. https://doi.org/10.1007/s12031-015-0518-5.

[46] Yang, L., Qi, Y., Yang, Y., 2015. Astrocytes control food intake by inhibiting AGRP neuron activity via adenosine A1 receptors. Cell Reports 11(5):798–807. https://doi.org/10.1016/j.celrep.2015.04.002.

[47] Weber, B., Barros, L.F., 2015. The astrocyte: powerhouse and recycling center. Cold Spring Harbor Perspectives in Biology 7(12):1–15. https://doi.org/10.1101/cshperspect.a020396.

[48] Rinholm, J.E., Vervaeke, K., Tadross, M.R., Tkachuk, A.N., Kopek, B.G., Brown, T.A., et al., 2016. Movement and structure of mitochondria in oligodendrocytes and their myelin sheaths. Glia 64(5):810–825. https://doi.org/10.1002/glia.22965.

[49] Stephen, T.-L., Higgs, N.F., Sheehan, D.F., Al Awabdh, S., Lopez-Domenech, G., Arancibia-Carcamo, I.L., et al., 2015. Miro1 regulates activity-driven positioning of mitochondria within astrocytic processes apposed to synapses to regulate intracellular calcium signaling. Journal of Neuroscience 35(48):15996–16011. https://doi.org/10.1523/JNEUROSCI.2068-15.2015.

[50] Motori, E., Puyal, J., Toni, N., Ghanem, A., Angeloni, C., Malaguti, M., et al., 2013. Inflammation-induced alteration of astrocyte mitochondrial dynamics requires autophagy for mitochondrial network maintenance. Cell Metabolism 18(6):844–859. https://doi.org/10.1016/j.cmet.2013.11.005.

[51] Agarwal, A., Wu, P.-H., Hughes, E.G., Fukaya, M., Tischfield, M.A., Langseth, A.J., et al., 2017. Transient opening of the mitochondrial permeability transition pore induces microdomain calcium transients in astrocyte processes. Neuron 93(3). https://doi.org/10.1016/j.neuron.2016.12.034, 587–605.e7.

[52] Jackson, J.G., Robinson, M.B., 2018. Regulation of mitochondrial dynamics in astrocytes: mechanisms, consequences, and unknowns. Glia 66(6):1213–1234. https://doi.org/10.1002/glia.23252.

[53] Filichia, E., Hoffer, B., Qi, X., Luo, Y., 2016. Inhibition of Drp1 mitochondrial translocation provides neural protection in dopaminergic system in a Parkinson's disease model induced by MPTP. Scientific Reports 6(1):32656. https://doi.org/10.1038/srep32656.

[54] Wang, Q., Zhang, M., Torres, G., Wu, S., Ouyang, C., Xie, Z., et al., 2017. Metformin Suppresses diabetes-accelerated atherosclerosis via the inhibition of Drp1-mediated mitochondrial fission. Diabetes 66(1):193–205. https://doi.org/10.2337/db16-0915.

[55] Li, G., Zhou, J., Budhraja, A., Hu, X., Chen, Y., Cheng, Q., et al., 2015. Mitochondrial translocation and interaction of cofilin and Drp1 are required for erucin-induced mitochondrial fission and apoptosis. Oncotarget 6(3):1834–1849. https://doi.org/10.18632/oncotarget.2795.

[56] Wang, P., Wang, P., Liu, B., Zhao, J., Pang, Q., Agrawal, S.G., et al., 2015. Dynamin-related protein Drp1 is required for Bax translocation to mitochondria in response to irradiation-induced apoptosis. Oncotarget 6(26):22598–22612. https://doi.org/10.18632/oncotarget.4200.

[57] Lee, D.-S., Kim, J.-E., 2018. PDI-mediated S-nitrosylation of DRP1 facilitates DRP1-S616 phosphorylation and mitochondrial fission in CA1 neurons. Cell Death & Disease 9(9):869. https://doi.org/10.1038/s41419-018-0910-5.